European Journal of Pharmaceutical Sciences 78 (2015) 190–197

Contents lists available at ScienceDirect

European Journal of Pharmaceutical Sciences

journal homepage: www.elsevier.com/locate/ejps

QSAR study and conformational analysis of 4-arylthiazolylhydrazones derived from 1-indanones with anti-*Trypanosoma cruzi* activity

Guido J. Noguera [a], Lucas E. Fabian [a], Elisa Lombardo [b], Liliana Finkielsztein [a,*]

[a] Química Medicinal, Departamento de Farmacología, IQUIMEFA (UBA-CONICET), Facultad de Farmacia y Bioquímica, Universidad de Buenos Aires, Junín 956, 1113 Ciudad Autónoma de Buenos Aires, Argentina

[b] Centro de Investigaciones sobre Porfirinas y Porfirias (CIPYP, UBA-CONICET), Hospital de Clínicas José de San Martín, Avenida Córdoba 2351, 1120 Ciudad Autónoma de Buenos Aires, Argentina

ARTICLE INFO

Article history:
Received 26 May 2015
Received in revised form 15 July 2015
Accepted 20 July 2015
Available online 22 July 2015

Keywords:
Chagas disease
Thiazolylhydrazones
Anti-trypanosomal activity
QSAR
Conformational analysis

ABSTRACT

A set of 4-arylthiazolylhydrazones derived from 1-indanones (TZHs) previously synthesized and assayed against *Trypanosoma cruzi*, the causative agent of Chagas disease, were explored in terms of conformational analysis. We found that TZHs can adopt four minimum energy conformations: *cis* (A, B and C) and *trans*. The possible bioactive conformation was selected by a 3D-QSAR model. Different molecular parameters were calculated to produce QSAR second-generation models. These QSAR results are discussed in conjunction with conformational analysis from molecular modeling studies. The main factor to determine the activity of the compounds was the partial charge at the N(3) atom (q_{N3}). The predictive ability of the QSAR equations proposed was experimentally validated. The QSAR models developed in this study will be helpful to design novel potent TZHs.

1. Introduction

Chagas disease, also called American trypanosomiasis, is a vector-transmitted parasitic disease caused by the flagellated protozoan microorganism *Trypanosoma cruzi* (*T. cruzi*). It is the third largest disease burden in Latin America after malaria and schistosomiasis, all considered as neglected diseases (WHO, 2008). The World Health Organization estimates that Chagas disease is responsible for the death of over 10,000 people per year (DNDI, 2008). At present, only two nitro derivative drugs, introduced in the 1960s and 1970s, are available for the treatment of chagasic patients: nifurtimox and benznidazole. These drugs are effective for acute infections, but their undesirable side effects and controversial use for chronic patients have been forcing the abandonment of the treatment (Urbina and Docampo, 2003; McKerrow et al., 2009). Moreover, no effective vaccines are available and their development in the near future seems to be out of reach (Vazquez-Chagoyan et al., 2011). Consequently, more efficient drugs are needed.

Recently, in continuation of our search for bioactive molecules, we envisaged that the thiazolylhydrazone moiety would generate novel templates which are likely to exhibit anti-*T. cruzi* activity. Thus, we prepared seventeen 4-arylthiazolylhydrazones derived from 1-indanones (TZHs) in an efficient and simple manner. Most of these new derivatives exhibited promising activity against the different forms of *T. cruzi* and were more potent and selective than the reference drug benznidazole (Caputto et al., 2012). A preliminary analysis of the structure–activity relationship suggested that better trypanocidal activity may be attained when R_1, R_2 or R_3 is a methyl group (Fig. 1).

Quantitative structure–activity relationship (QSAR) is one of the most important areas in chemometrics, and is a valuable tool extensively used in drug design and medicinal chemistry. Thus, in this work, we performed a QSAR study with the aim to explore the controlling factors governing the observed pharmacological properties of TZHs and to predict the biological activities of new compounds. Furthermore, an exhaustive conformational analysis was performed to obtain more precise representation of the biological active molecules at the atomic level. Also, three new TZHs are described.

2. Materials and methods

2.1. Chemistry

Melting points (uncorrected) were determined on a Thomas Hoover apparatus. Thin layer chromatography (TLC) was used to

* Corresponding author.
E-mail address: lfinkiel@ffyb.uba.ar (L. Finkielsztein).

http://dx.doi.org/10.1016/j.ejps.2015.07.014
0928-0987/

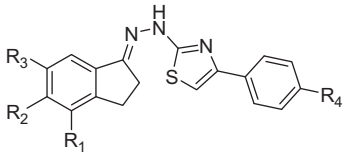

Fig. 1. General structure of 4-arylthiazolylhydrazones derived from 1-indanones (TZHs).

monitor reactions. Reactions were carried out in a Microwave Synthesis Reactor Microwave 300 Anton Paar. IR spectra were recorded as KBr pellets using a Perkin Elmer Spectrum One FT-IR spectrophotometer. ^{1}H and ^{13}C NMR spectra were recorded on a Bruker 500 MHz spectrometer. High resolution mass spectra were acquired on a Bruker micrOTOF-Q II spectrometer. 4-Methoxy-phenacyl bromide and 4-nitro-phenacyl bromide were purchased from Sigma–Aldrich and used as received. 4-Fluor-phenacyl chloride and thiosemicarbazones derived from 1-indanones were prepared according to the protocols previously described (Caputto et al., 2012, 2011; Finkielsztein et al., 2008).

2.1.1. General procedure for the synthesis of 4-arylthiazolylhydrazones derived from 1-indanones

In a typical procedure a mixture of thiosemicarbazone derived from 1-indanone (0.010 mmol), phenacyl chloride or bromide (0.013 mmol) and DMF (0.15 mL) in a borosilicate boiling tube, was placed in a microwave synthesizer at 80 °C. After completion of the reaction (monitored by TLC), the mixture was suspended in water, filtered, and washed with EtOH and hexane. All synthesized TZHs were crystallized from EtOH.

2.1.1.1. 4-(4-fluorophenyl)-2-(2-(6-methyl-2,3-dihydro-1H-inden-1-ylidene)hydrazinyl)thiazole (18). Yield: 73%. Mp: 216-217 °C. IR ν/cm^{-1} (KBr): 2615 (NH^{+}), 1621 and 1598 (C=N). ^{1}H NMR (DMSO-d_6): δ: 2.34 (3H, s, CH_3), 2.87 (2H, m, CH_2), 3.02 (2H, m, CH_2), 7.17 (1H, d, J = 7.8 Hz, H-Ar), 7.23 (2H, t, J = 8.9 Hz, H-Ar), 7.25 (1H, d, J = 7.8 Hz, H-Ar), 7.28 (1H, s, H-thiazole), 7.42 (1H, s, H-Ar), 7.89 (2H, dd, J_1 = 5.5 Hz, J_2 = 8.9 Hz, H-Ar), 11.13 (1H, s, NH). ^{13}C NMR (DMSO-d_6): 20.8, 27.7, 27.9, 103.5, 115.3, 115.5 (J = 21.8 Hz), 120.8, 125.4, 127.4, 127.6 (J = 8.2 Hz), 131.1, 131.4, 136.2, 137.8, 145.2, 149.8, 156.4, 160.6, 162.6 (J = 244.3 Hz), 169.5. HRMS (ESI) m/z $(M+H)^{+}$ calcd for $C_{19}H_{17}FN_3S$ 338.11217, found 338.11035.

2.1.1.2. 4-(4-methoxyphenyl)-2-(2-(5-methyl-2,3-dihydro-1H-inden-1-ylidene)hydrazinyl)thiazole (19). Yield: 99%. Mp: descompose before melting. IR ν/cm^{-1} (KBr): 2765 (NH^{+}), 1624 and 1583 (C=N). ^{1}H NMR (DMSO-d_6): δ: 2.33 (3H, s, CH_3), 2.86 (2H, m, CH_2), 3.03 (2H, m, CH_2), 3.77 (3H, s, OCH_3), 6.96 (2H, d, J = 8.8 Hz, H-Ar), 7.11 (1H, s, H-thiazole), 7.12 (1H, d, J = 7.8 Hz, H-Ar), 7.18 (1H, s, H-Ar), 7.50 (1H, d, J = 7.8 Hz, H-Ar), 7.78 (2H, d, J = 8.8 Hz, H-Ar), 11.05 (1H, s, NH). ^{13}C NMR (DMSO-d_6): 21.2, 27.7, 28.0, 55.1, 101.5, 114.0, 120.5, 126.1, 126.5, 126.9, 128.0, 135.1, 135.6, 139.9, 148.2, 158.8, 159.2, 169.5. HRMS (ESI) m/z $(M+H)^{+}$ calcd for $C_{20}H_{20}N_3OS$ 350.13216, found 350.13162.

2.1.1.3. 2-(2-(5-methyl-2,3-dihydro-1H-inden-1-ylidene)hydrazinyl)-4-(4-nitrophenyl)thiazole (20). Yield: 92%. Mp: 241-242 °C. IR ν/cm^{-1} (KBr): 2742 (NH^{+}), 1597 (C=N), 1566 and 1335 (NO_2). ^{1}H NMR (DMSO-d_6): δ: 2.33 (3H, s, CH_3), 2.86 (2H, m, CH_2), 3.04 (2H, m, CH_2), 7.12 (1H, d, J = 7.9 Hz, H-Ar), 7.18 (1H, s, H-Ar), 7.50 (1H, d, J = 7.9 Hz, H-Ar), 7.69 (1H, s, H-thiazole), 8.11 (2H, d, J = 8.9 Hz, H-Ar), 8.27 (2H, d, J = 8.9 Hz, H-Ar), 11.16 (1H, s, NH). ^{13}C NMR (DMSO-d_6): 21.2, 27.7, 28.0, 108.5, 120.5, 124.1, 126.1, 126.3, 128.0, 135.1, 139.9, 140.9, 146.1, 148.3, 148.6, 156.7, 169.9. HRMS (ESI) m/z $(M+H)^{+}$ calcd for $C_{19}H_{17}N_4O_2S$ 365.10667, found 365.10675.

2.2. Biology

2.2.1. Parasites

T. cruzi epimastigotes (Tulahuen strain, Tul 2 stock) were grown at 28 °C in a liquid medium containing 0.3% yeast extract, 0.9% tryptose, 0.4% dextrose, 1% disodium phosphate 2-hydrate, 0.36% sodium chloride, 0.04% potassium chloride, 0.15% powered beef liver, 0.5% brain heart infusion and 0.5–1.0 mg/100 mL hemin.

2.2.2. In vitro trypanocidal activity assay

To evaluate the growth inhibition of *T. cruzi* epimastigote, parasites from a 5 days-old culture were inoculated into fresh culture medium to reach an initial concentration of 1.5–2.5 × 10^6 cells/mL. Cells were cultured with different concentrations of compounds (usually of 1.50–15 μM or 0.5–2.5 μM) for 4 days. Benznidazole (2.50–15 μM) was used as the reference trypanocidal drug (positive control). The compounds ability to inhibit growth of the parasite (antiproliferative activity) was evaluated, in triplicate, in comparison to the control without drug. Cells growth was followed by counting the number of cells per mL of culture using a Neubauer chamber and was expressed as cellular density (CD). For the count only the cells showing motility (parasites without motility were dead as demonstrated by positive staining with trypan blue) were taking into account. The percentage of inhibition (%I) was calculated as: $\%I = \{1-[(CD_{5t} - CD_{0t})/(CD_{5c} - CD_{0c})]\} \times 100$, where CD_{5t} is cellular density of treated parasites at day 5; CD_{0t} is cellular density of treated parasites just immediately after adding the drug (day 0); CD_{5c} is cellular density of untreated parasites (control) at day 5; and CD_{0c} is cellular density of untreated parasites at day 0. The IC_{50} (50% inhibitory concentration on epimastigote forms) was estimated by lineal regression analysis from the %I values and the decimal logarithm (log) of drug concentration.

2.3. Computational methods

2.3.1. Molecular modeling methods

The initial conformations (IC) of the compounds were drawn by means of the "Model Build" modulus of the HyperChem 8.0.7 (Hypercube, 2009). The molecular structures were pre-optimized with the MM+ procedure included in the HyperChem software. The resulting geometries were refined by means of the AM1 semiempirical Method from the Molecular Orbitals Theory, setting the calculation of the Self Consistent Field (SCF) with a convergence limit equal to 1 × 10^{-7} and iteration limit equal to 1000, using the Polak–Ribiere algorithm and a RMS gradient norm limit of 0.001 kcal $Å^{-1}$ mol. The lowest energy conformer of each compound was corroborated by vibrational analysis. Full geometry optimization of minimum energy conformations was subsequently carried out at the HF/6-31G(d) *ab initio* level using Gaussian 09 (Gaussian Inc, 2009). The study of the structural conformers was performed using Balloon 1.3.1.983 software (Vainio and Johnson, 2007). This software generates conformational ensembles (CEs) employing the multiobjective genetic algorithm (GA) together with the MMFF94 force field and was configured with the following options: *fullforce* (optimization of the found post-GA conformations), *nconfs* = 90 (initial population size), *nGenerations* = 500 (maximum number of generations) and *keepinitial* (output file including the IC). Molecular descriptors were calculated with the PaDEL-descriptor 2.11 software (Yap, 2011).

2.3.2. QSAR settings

The construction of QSAR equations was performed by McQSAR software (Vainio and Johnson, 2005) using the GA to create

statistical models based on a calibration data set. The program was setting as follows: (a) GA to evolved equations: *collinearity cutoff* = 0.5, *popSize* = 100, *generationSize* = 1024, *nGenerations* = 5, *tournamentSize* = 3, *pMutation* = 0.03. (b) GA to evolved conformation: *popSize* = 100, *generationSize* = 1000, *nGenerations* = 10, *tournamentSize* = 3, *pMutation* = 0.1.

3. Results and discussion

3.1. Chemistry

The synthetic pathway for the preparation of the new TZHs **18**–**20** (depicted in Scheme 1) is based on the method previously described by us for the synthesis of TZHs **1**–**17** (Caputto et al., 2012). The new compounds were obtained from the reaction of the thiosemicarbazone of 1-indanones conveniently substituted and the corresponding phenacyl halides. Since the presence of methyl group at R_1, R_2 or R_3 is necessary for an optimal anti-*T. cruzi* activity, the main structural diversity stems from the *para* substituents (R_4 group). New derivatives were obtained in high yields and the structure of compounds was confirmed by ^1H and ^{13}C NMR, IR and HRMS data. The general structure of the TZHs studied is shown in Table 1.

3.2. In vitro anti-T. cruzi activity

The new compounds, **18**–**20**, were biologically evaluated in aqueous solutions obtained from stock solutions of the TZHs in DMSO, whose final concentration did not exceed 1% DMSO. These TZHs were tested in vitro against the epimastigote form of *T. cruzi*, Tulahuen 2 strain. Compounds **18**–**20** were incorporated into the media at the following concentrations: 15, 10, 7.5, 5 and 2.5 μM. Table 1 shows the IC_{50} (50% inhibitory concentration) value determined for all TZHs (**1**–**20**). Benznidazole was used as the reference trypanosomicidal agent. Compounds **18** and **20** displayed moderate activities, while TZH **19** resulted more active than the reference drug (IC_{50} = 4.16 ± 0.12 μM) and with an activity value similar to those of the most active TZHs previously synthesized.

Table 1
TZHs synthesized and their biological characterization against the epimastigote form of *T. cruzi*.

TZHs	R_1	R_2	R_3	R_4	IC_{50}[b, c] (μM)
1[a]	H	H	H	H	18.99 ± 2.59
2[a]	H	H	H	CH_3	>15
3[a]	H	H	H	Cl	8.62 ± 0.25
4[a]	H	OCH_3	OCH_3	H	10.14 ± 0.43
5[a]	H	OCH_3	OCH_3	CH_3	>15
6[a]	H	OCH_3	OCH_3	Cl	7.17 ± 0.56
7[a]	CH_3	H	H	H	7.08 ± 0.68
8[a]	CH_3	H	H	CH_3	4.36 ± 0.49
9[a]	CH_3	H	H	Cl	4.53 ± 0.66
10[a]	OCH_3	H	H	Cl	11.78 ± 0.55
11[a]	NO_2	H	H	Cl	17.05 ± 0.78
12[a]	H	CH_3	H	Cl	7.15 ± 0.53
13[a]	H	H	CH_3	Cl	8.59 ± 0.65
14[a]	H	CH_3	H	H	4.69 ± 0.43
15[a]	H	CH_3	H	CH_3	5.24 ± 0.27
16[a]	H	H	CH_3	H	4.27 ± 0.24
17[a]	H	H	CH_3	CH_3	4.08 ± 0.20
18	H	H	CH_3	F	7.81 ± 0.71
19	H	CH_3	H	OCH_3	4.16 ± 0.12
20	H	CH_3	H	NO_2	5.39 ± 0.30
Benznidazole					5.39 ± 0.25

[a] Caputto et al., 2012.
[b] IC_{50}: concentration (in μM) that inhibits 50% of epimastigote form of *T. cruzi* growth.
[c] All data are expressed as means ± standard deviations of three separate experiments, running in duplicates or triplicates.

3.3. QSAR study

3.3.1. Anti-T. cruzi activity

The IC_{50} value of each compound was converted to pIC_{50} ($-\log IC_{50}$) and used as dependent variable for the development of valid QSAR models.

3.3.2. Descriptors

Molecular descriptors represent the way in which the chemical information contained in the molecular structure is transformed and coded to deal with chemical, pharmacological and toxicological problems in QSAR studies. A series of 1D, 2D and 3D molecular descriptors were used to characterize each CE in terms of their lipophilicity, connectivity index, topology, mass distribution and polar surface. Weighted Holistic Invariant Molecular (WHIM) descriptors, which contain information about whole molecular structure in terms of size, shape, symmetry and atom distribution, were also included in this characterization (Todeschini and Consonni, 2009). WHIM descriptors are calculated by a principal component analysis (PCA) on the centered Cartesian coordinates of the atoms weighted according to different weighting schemes: atomic masses (mass), unitary weights (unity), van der Waals volumes (vol.), Mulliken atomic electronegativities (mull.), atomic polarizabilities (pol.) and electrotopological indexes (s). Directional and nondirectional WHIM descriptors can be calculated. Directional WHIM descriptors are univariate statistical indexes which are calculated from the scores of each individual principal component (1, 2, 3), related to molecular size ($\lambda 1$, $\lambda 2$, $\lambda 3$), shape ($\theta 1$, $\theta 2$), symmetry ($\gamma 1$, $\gamma 2$, $\gamma 3$), and density of atom distribution ($\eta 1$, $\eta 2$, $\eta 3$). Non-directional WHIM indexes, easily obtained from directional ones, bear global information about molecular size (T, A, and V), shape (K), symmetry (G), and density (D).

3.3.3. QSAR model

The QSAR study was performed using the McQSAR software (Vainio and Johnson, 2005). This software program is able to use descriptors for multiple representations per compound, such as different conformers. Fifteen TZHs (**1**, **3**, **4**, **6**–**17**) were used for the present QSAR modeling. Compounds **2** and **5** were not included because their IC_{50} values were not defined (IC_{50} > 15 μM). Multiple linear regression analysis was used to search for optimal QSAR

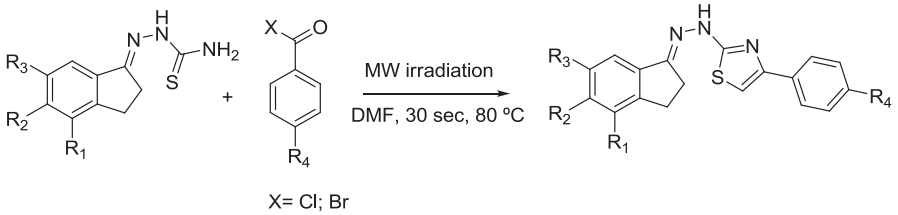

Scheme 1. Synthesis of TZHs by condensation of 1-indanone thiosemicarbazone derivatives and phenacyl halides.

models that were able to correlate molecular descriptors with the bioactivity variation across the set of compounds used. Eq. (1) represents our best performing QSAR model and Fig. 2 shows the corresponding scatter plot of the estimated versus experimental activity values for the fifteen TZHs, against the epimastigote form of *T. cruzi*.

$$\begin{aligned} &\mathrm{pIC_{50}} = 5.25 + 0.22 \times W\lambda 1.u - 0.89 \times W\eta 3.\mathrm{e} \\ &n = 15, R^2 = 0.872, \mathrm{SD} = 0.083, F = 40.74 \end{aligned} \quad (1)$$

(Here and thereafter, n = number of data points, R^2 = square correlation coefficient, SD = standard error of the estimate and F = Fisher statistics). Where $W\lambda$1.u is a geometric directional WHIM descriptor and $W\eta$3.e is an electronic directional WHIM descriptor. The inclusion of directional WHIM descriptors in the model suggested that the placement of certain atoms in the molecular skeleton influences the anti-*T. cruzi* activity.

Taking into account that the geometric directional WHIM descriptor included in Eq. (1) encodes information about the spatial arrangement of the molecule, we performed an exhaustive investigation of the structural parameters based on the conformations of TZHs selected by the McQSAR software. Interestingly, we observed that the value of the dihedral angle Φ_1 = C(1)═N(2)─NH(3)─C(4) (Fig. 3A) was highly correlated with the value of the $W\lambda$1.u descriptor, and hence with the anti-*T. cruzi* activity. Thus, the more active TZHs (IC_{50} between 4 to 8 μM) possess the highest Wλ1.u values (1.282–2.311), which correlate with Φ_1 values around 90°. In contrast, the less active TZHs (IC_{50} > 10 μM) have the lowest $W\lambda$1.u values (0.148–0.198), which correlate with Φ_1 values around 180° (Table 2).

Since the values of the angle Φ_1 considered are derived from the CEs, which were calculated by the Balloon software (through its force field MMFF94), then a full geometry optimization of the conformations selected by the McQSAR software was subsequently carried out at the HF/6-31G(d) *ab initio* level, using Gaussian 09 (Gaussian Inc, 2009). Each conformer was energy-optimized using restraints for dihedral angles, allowing the rest of the molecule to be minimized. Additionally, the resulting conformations were re-minimized without restraints. Both optimized structures (with restraints and without restraints) showed to be energetically similar (Supplementary file 1), and the values of the dihedral angle considered differed only about 6–21°. Consequently, the conformations selected to calculate the QSAR model were energetically probable and consistent with minimum energy conformations.

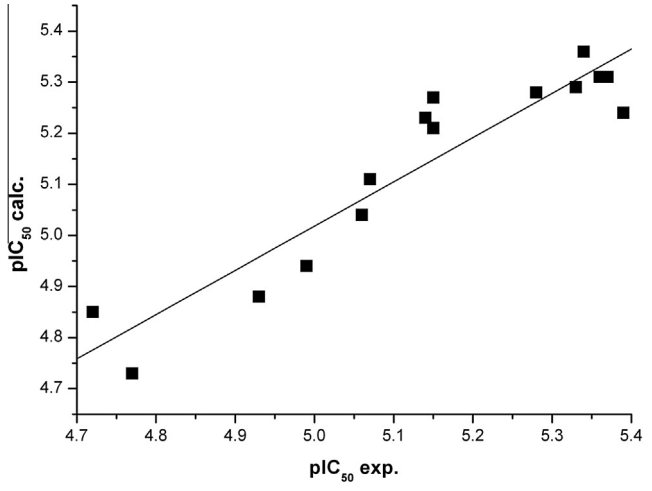

Fig. 2. Linear regression of calculated versus experimental pIC_{50} values from Eq. (1).

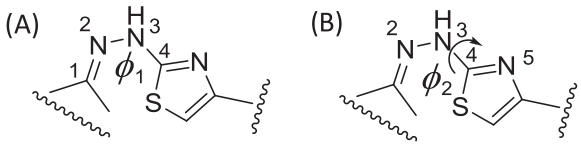

Fig. 3. (A) Atoms involved in the dihedral angle Φ_1 = C(1)═N(2)─NH(3)─C(4); (B) Atoms involved in the dihedral angle Φ_2 = N(2)─NH(3)─C(4)═N(5).

Table 2
IC_{50} values of TZHs and values of the dihedral angle Φ_1 and $W\lambda$1.u of the conformations selected from Eq. (1).

TZHs[a]	IC_{50} (μM)	$W\lambda$1.u	Dihedral angle Φ_1 (degrees)
17	4.08 ± 0.20	1.926	92
16	4.27 ± 0.24	1.955	101
8	4.36 ± 0.49	1.677	105
9	4.53 ± 0.66	1.613	95
14	4.69 ± 0.43	1.391	95
15	5.24 ± 0.27	1.372	94
7	7.08 ± 0.68	1.621	95
12	7.15 ± 0.53	1.282	106
6	7.17 ± 0.56	2.311	93
13	8.59 ± 0.65	1.793	105
3	8.62 ± 0.25	1.466	95
4	10.14 ± 0.43	**0.198**	**180**
10	11.78 ± 0.55	**0.173**	**180**
11	17.05 ± 0.78	**0.156**	**179**
1	18.99 ± 2,59	**0.148**	**180**

[a] TZHs are sorted in descending order of activity.

3.4. Conformational analysis

In order to have an approach to the preferred conformation that TZHs adopt during the interaction with their potential target, we carried out a systematic conformational search analysis. Firstly, we studied the rotation of the dihedral angle Φ_2 = N(2)─NH(3)─C(4)═N(5) from 0° to 355° at intervals of 5° (Fig. 3B). Each resulting conformation was minimized at the HF/6-31G(d) *ab initio* level, using Gaussian 09. The conformational energy surfaces for TZH **1** are shown in Fig. 4a. This rotation yielded two minimum energy conformations: *cis* (I), with the N(2) atom in the same side as the N(5) atom, and *trans* (II), with the N(2) atom in the opposite side of the N(5) atom. The same patterns of energy surfaces were observed for all the TZHs under study. To estimate the energetic barrier between conformations I and II, the structures were analyzed at the second-order Møller–Plesset perturbation theory (MP2). The results of frequency calculations of this theory are more reliable, such that the optimized geometries are characterized by harmonic vibrational frequencies, which confirmed that the structures obtained are minimal on the potential-energy surface (Parr and Yang, 1989). The conformation of maximum energy was minimized by using the "Berny algorithm", which uses the forces acting on the atoms of a given structure together with the second derivative matrix (called the Hessian matrix) to predict energetically more favorable structures and thus optimize the molecular structure toward the next local minimum on the potential energy surface. The energy barrier estimated was 9.04 Kcal/mol, indicating a considerable restriction for the free rotation of the dihedral angle considered.

Subsequently, each minimum energy conformation (I and II) was analyzed by the rotation of the dihedral angle Φ_1 = C(1)═N(2)─NH(3)─C(4). The conformational energy surfaces are shown in Fig. 4B. From conformation II, only one minimum (around 180°) was observed (Fig. 4B.1). In contrast, conformation I was able to adopt three minimum energy conformations, named by us: A (Φ_1 around 85°), in which the indanic nucleus is below the

phenylthiazolylhydrazone plane; B (Φ_1 around 180°), in which the molecule adopts a planar disposition; and C (Φ_1 around −85°), in which the indanic nucleus is above the phenylthiazolylhydrazone plane (Fig. 4B.2). The preceding results suggest that conformation I is more flexible than conformation II. The energy barrier between A and B or B and C, calculated as above, is 4.59 Kcal/mol, which indicates a certain probability of interconversion.

Reviewing the conformations of the TZHs selected by the McQSAR software in the QSAR analysis, it can be seen that the more active compounds possess a *cis* conformation (I C) with a Φ_1 value around -85°. In contrast, the less active compounds possess a *trans* conformation with a Φ_1 value around 180° (Fig. 5).

3.5. Electronic properties

Taking into account that the antitrypanosomal activity is dependent on both geometric and electronic properties (Eq. (1)), to depict a more reliable electronic structure characterization some global descriptors, such as frontier molecular orbital energies (*E*HOMO, *E*LUMO), dipole moments (μ), Mulliken charge distribution, Natural Bond Orbital (NBO), Restrained Electrostatic Potential (RESP) atomic partial charges (q) and the molecular electrostatic potential (MEP), were determined from the HF/6-31G(d) *ab initio* level calculation using Gaussian 09 software and analyzed (Supplementary file 2). Table 3 shows RESP atomic partial charges at the N(3) and N(5) atom (q_{N3} and q_{N5}, respectively).

The calculated values of the electronic properties reveal no correlation between the computed parameters and the anti-*T. cruzi* activity. However, the thiazolylhydrazone moiety showed a quite different distribution of charge, particularly evident in the case of q_{N3} (Table 3). Thus, the more active TZHs (**3**, **6**, **7**, **8**, **9**, **12**, **13**, **14**, **15**, **16** and **17**) possessed a more negative value of q_{N3} (between −0.628 and −0.735), suggesting that this atom is more exposed to electrophilic attacks and probably plays an essential role in interactions with an active site. Consistent with this observation, the less active compounds (**1**, **4**, **10** and **11**) had a less negative value of q_{N3} (between −0.214 and −0.400). On the other hand, the more active TZHs showed less negative values of q_{N5}.

To explore the interaction capabilities of TZHs, the MEP diagrams were explored for this series of compounds in the minimum energy conformations selected by the McQSAR software. Fig. 6 compares the MEP contour map distribution for some representative TZHs. The negative electrostatic potential corresponds to the attraction of a proton by the concentrated electron density in the molecule (lone pairs, pi-bonds), thus revealing sites for electrophilic attack (colored in shades of red in standard contour diagrams). The negative region is mainly localized around the N(3) atom, being the most reactive part in the molecule for more active TZHs. Interestingly, this particular region is observed only when

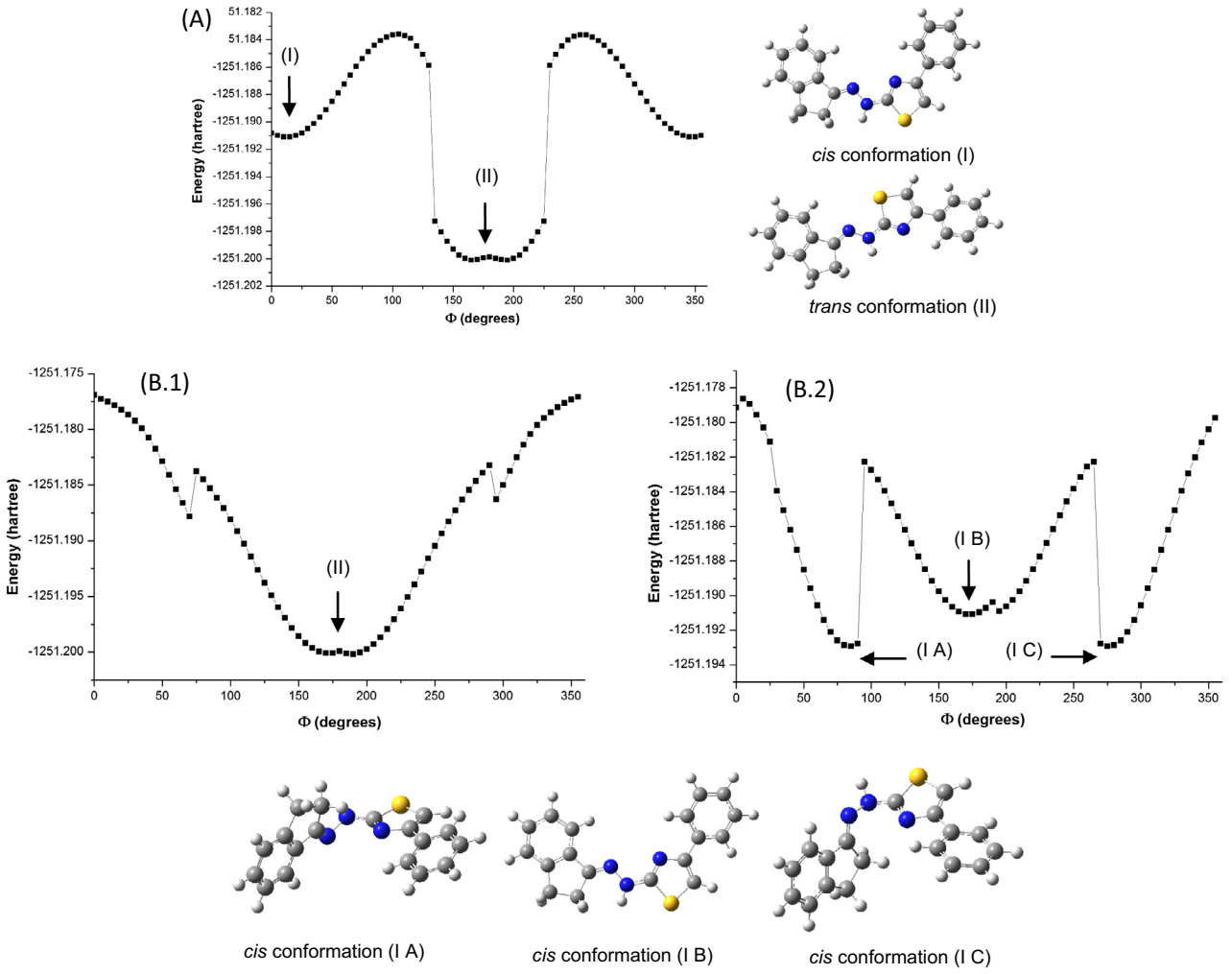

Fig. 4. (A) Conformational energy surface and minimum energy conformations for TZH **1** obtained from the rotation of the dihedral angle Φ_2; (B.1) Conformational energy surface and minimum energy conformations for TZH **1** (*trans* conformation II) obtained from the rotation of the dihedral angle Φ_1; (B.2) Conformational energy surface and minimum energy conformations for TZH **1** (*cis* conformation I) obtained from the rotation of the dihedral angle Φ_1.

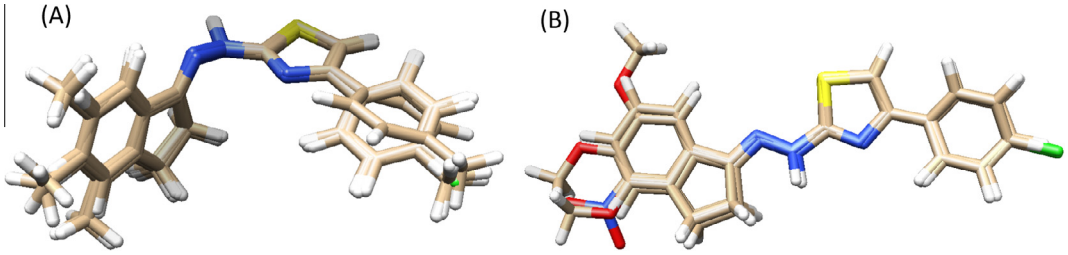

Fig. 5. (A) Superimposition for the *cis* (I C) conformation of the more active TZHs (**8**, **9**, **14**, **15**, **16**, **17**); (B) Superimposition for the *trans* (II) conformation of the less active TZHs (**1**, **4**, **10**, **11**).

Table 3
Electronic properties of TZHs: RESP atomic partial charges at the N(3) atom (q_{N3}) and the N(5) atom (q_{N5}).

TZHs[a]	IC_{50}(μM)	q_{N3}	q_{N5}
17	4.08	−**0.678**	−0.397
16	4.27	−**0.706**	−0.375
8	4.36	−**0.711**	−0.377
9	4.53	−**0.733**	−0.394
14	4.69	−**0.695**	−0.390
15	5.24	−**0.649**	−0.358
7	7.08	−**0.719**	−0.422
12	7.15	−**0.683**	−0.363
6	7.17	−**0.628**	−0.338
13	8.59	−**0.678**	−0.350
3	8.62	−**0.693**	−0.400
4	10.14	−0.323	−0.594
10	11.78	−0.400	−0.620
11	17.05	−0.390	−0.621
1	18.99	−0.214	−0.606

[a] TZHs are sorted in descending order of activity.

TZHs adopt *cis* conformation (Φ_1 around −85°). Hence, the spatial arrangement modifies the electronic distribution of the thiazolyl-hydrazone function. These findings support the hypothesis that the anti-*T. cruzi* activity of TZHs is closely related to the ability of the N(3) atom to interact with a potential target. This condition occurs when the compounds adopts *cis* C conformantion. Finally, *cis* C seems to be the pharmacologically active conformation.

3.6. Second-generation QSAR models

With the aim to predict the activity of novel compounds, we explored the generation of new QSAR models that would better take into account the conformations of the TZHs studied. Thus, the fifteen TZHs (**1**, **3**, **4**, **6**–**17**) were used as a training set and were re-minimized using Gaussian 09 HF/6-31G(d) at the *cis* conformation named C. Different partial charge methods were calculated (Mulliken, NBO and RESP). Besides, the indanic nucleus and phenyl substituents included in the structure of each TZH were optimized by means of the AM1 semiempirical method from the Molecular

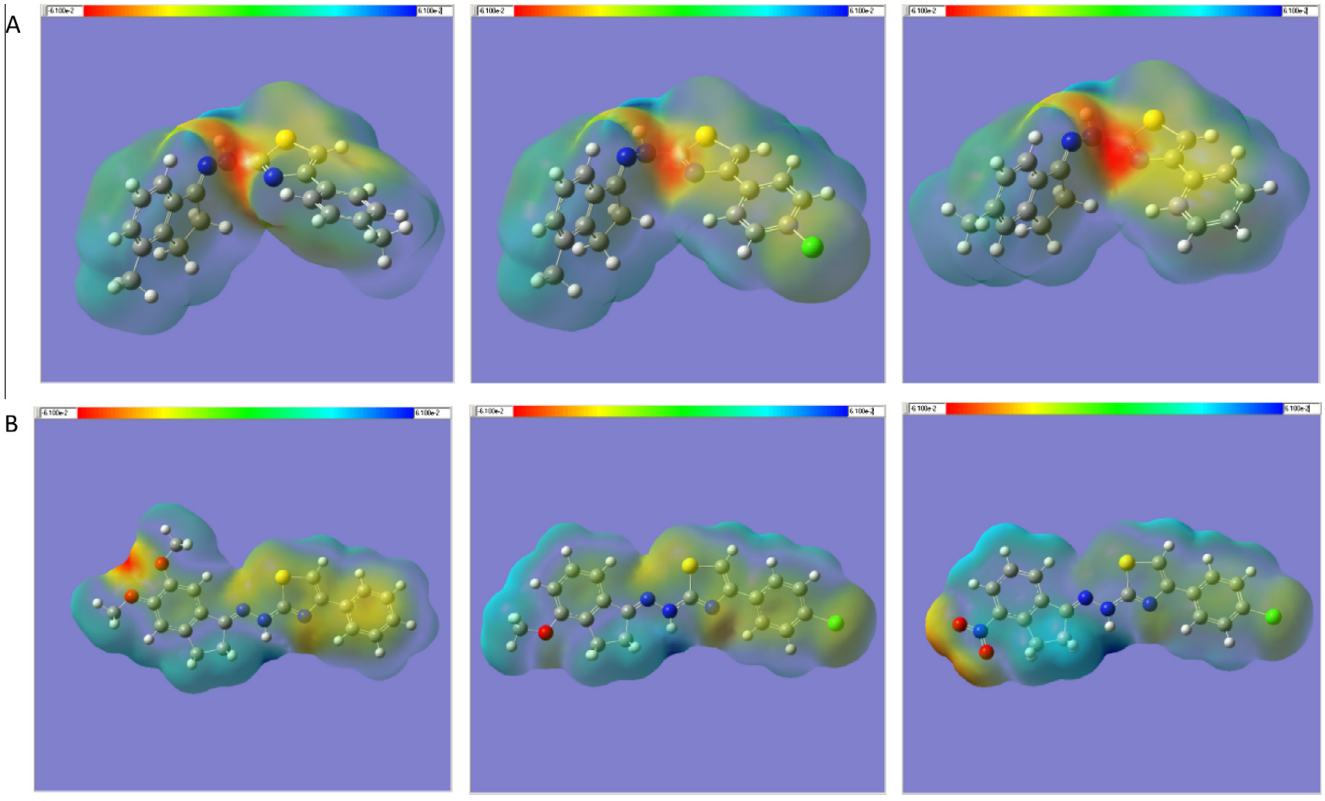

Fig. 6. MEP contour map distribution for: (A) TZHs **8**, **9** and **14** (*cis* conformation (I C)); B) TZHs **4**, **10** and **11** (*trans* conformation).

Table 4
Observed and calculated anti-*T. cruzi* activity of the training set and the test set according to QSAR Eqs. 3 and 4.

TZHs	pIC_{50} exp	Eq. (3)		Eq. (4)	
		pIC_{50} calc	Residuals	pIC_{50} calc	Residuals
Training set					
1	4.72	4.78	−0.06	4.83	−0.11
3	5.06	5.07	−0.01	5.03	0.04
4	4.99	4.94	0.05	5.01	−0.02
6	5.14	5.16	−0.01	5.14	0.01
7	5.15	5.33	−0.18	5.33	−0.18
8	5.36	5.33	0.03	5.42	−0.06
9	5.34	5.38	−0.04	5.29	0.05
10	4.93	4.94	−0.01	4.92	0.01
11	4.77	4.79	−0.02	4.76	0.01
12	5.15	5.17	−0.02	5.10	0.04
13	5.07	5.26	−0.19	5.20	−0.14
14	5.33	5.27	0.05	5.29	0.04
15	5.28	5.21	0.07	5.30	−0.02
16	5.37	5.21	0.15	5.22	0.15
17	5.39	5.25	0.13	5.34	0.05
Test set					
2	4.82	4.78	0.04	4.92	−0.10
5	4.82	5.01	−0.19	5.16	−0.34
18	5.11	5.11	0.00	5.40	−0.29
19	5.38	5.18	0.20	5.31	0.07
20	5.27	5.36	−0.09	5.26	0.01

Orbitals Theory included in Hyperchem 8.0.7, and different parameters were calculated by means of the QSAR properties modulus. The predictive linear QSAR reported in Eq. (2) establishes a link between the IC_{50} values and two descriptors: LogP_IND (partitioning coefficients corresponding to the indanic nucleus) and q_{N3} (RESP partial charge at the N(3) atom).

$$pIC_{50} = -7.02 \times q_{N3} + 0.60 \times \text{LogP\_IND} - 0.89$$
$$n = 15, R^2 = 0.702, \text{SD} = 0.127, F = 14.13 \quad (2)$$

The atomic charge at N(3) atom correlates with the activity observed. The regression equation indicates that the more negative q_{N3}, the larger the anti-*T. cruzi* activity. We noticed that the presence of electron-donating substituents in the indanic nucleus was related to more negative values of the atomic charge at N(3). Further, according to Eq. (2), the substituents must also be hydrophobic. These results are in coincidence with previous findings, where R_1, R_2 or R_3 = CH_3 were observed to increase the trypanocidal activity.

To investigate the role of the R_4 substituent in the phenyl ring, we determined Vol_R_4 (volume of the substituent R_4) and q_{CR4} (RESP atomic partial charge at C of the phenyl ring attached to R_4). The combination of these descriptors with the previous q_{N3} and LogP_IND improved the correlation equations for anti-*T. cruzi* activity, as can be seen in Eqs. 3 and 4.

$$pCI_{50} = -8.49 \times q_{N3} + 0.64 \times \text{LogP\_IND} + 0.0032 \times Vol\_R_4 - 1.97$$
$$n = 15, R^2 = 0.804, \text{SD} = 0.108, F = 15.09 \quad (3)$$

$$pCI_{50} = -8.02 \times q_{N3} + 0.55 \times LogP\_\text{IND} + 0.53 q_{CR4} - 1.30$$
$$n = 15, R^2 = 0.850, \text{SD} = 0.094, F = 20.73 \quad (4)$$

The QSAR models determined were externally validated using compounds **2** and **5** and the three new TZHs synthesized (**18**–**20**) (test set). The activities observed and those provided by the QSAR study for all TZHs are presented in Table 4. The correlation plots between the experimental and predicted data from the derived multiple regression QSAR Eqs. 3 and 4 are shown in Supplementary file 3. The calculated activities showed a correct fit. Therefore, the models developed can be successfully applied to predict the trypanocidal activity for new TZHs and new possible antichagasic candidates that still do not present experimentally assigned biological data. Furthermore, the application of the QSAR equations has a great importance in the virtual screening of new compounds before their synthesis, and thus represents an effective alternative in terms of time and economic aspects.

4. Conclusions

The QSAR study carried out to find the relationship between the physicochemical parameters of TZHs and their anti-*T. cruzi* activity indicated the importance of the spatial arrangement of the constituent atoms of TZHs. A more exhaustive investigation demonstrated high correlation between the anti-*T. cruzi* activity and the dihedral angle Φ_1 = C(1)═N(2)—NH(3)—C(4) value of the thiazolylhydrazone moiety. The conformational analysis of TZHs indicated that they can adopt four common minimum energy conformations: *trans* (Φ_1 around 180°) and *cis* A (Φ_1 around 85°), *cis* B (Φ_1 around 180°) and *cis* C (Φ_1 around −85°). We observed that the more active TZHs had *cis* C conformation according to the structures selected by the QSAR model, suggesting that *cis* C could be the pharmacological conformation. In addition, these compounds showed a more negative value of RESP atomic partial charges at N(3), indicating that this atom probably plays an essential role in the interactions with an active site. Taking into account the *cis* C conformation, the new QSAR models generated were able to predict the activity of TZHs that had not been contemplated during the development of the model. In summary, the results achieved in this work give new insights to improve the anti-*T. cruzi* profile of TZHs and could help to develop new antichagasic compounds.

Acknowledgments

We thank CONICET for scholarship to Guido J. Noguera. Financial supports from Universidad de Buenos Aires UBACYT B001 (2011–2014) 20020100100770 and (2014–2017) 200201130100005BA.

Appendix A. Supplementary material

Supplementary data associated with this article can be found, in the online version, at http://dx.doi.org/10.1016/j.ejps.2015.07.014.

References

Caputto, M.E., Fabian, L.E., Benitez, D., Merlino, A., Rios, N., Cerecetto, H., Moltrasio, G.Y., Moglioni, A.G., Gonzalez, M., Finkielsztein, L.M., 2011. Thiosemicarbazones derived from 1-indanones as new anti-*Trypanosoma cruzi* agents. Bioorg. Med. Chem. 19, 6818–6826.
Caputto, M.E., Ciccarelli, A., Frank, F., Moglioni, A.G., Moltrasio, G.Y., Vega, D., Lombardo, E., Finkielsztein, L.M., 2012. Synthesis and biological evaluation of some novel 1-indanone thiazolylhydrazone derivatives as anti-*Trypanosoma cruzi* agents. Eur. J. Med. Chem. 55, 155–163.
DNDi – Drugs for Neglected Disease Initiative, 2008..
Finkielsztein, L.M., Castro, E.F., Fabian, L.E., Moltrasio, G.Y., Campos, R.H., Cavallaro, L.V., Moglioni, A.G., 2008. New 1-indanone thiosemicarbazone derivatives active against BVDV. Eur. J. Med. Chem. 43, 1767–1773.
Gaussian Inc, Wallingford CT, 2009..
Hypercube Inc, Florida, 2009..
McKerrow, J.H., Doyle, P.S., Engel, J.C., Podust, L.M., Robertson, S.A., Ferreira, R., Saxton, T., Arkin, M., Kerr, I.D., Brinen, L.S., Craik, C.S., 2009. Two approaches to discovering and developing new drugs for Chagas disease. Mem. Inst. Oswaldo Cruz 104, 263–269.
Parr, R.G., Yang, W., 1989. Density-Functional Theory of Atoms and Molecules. Oxford University Press, New York.
Todeschini, R., Consonni, V., 2009. Molecular Descriptors for Chemoinformatics. Wiley-VCH, Weinheim, Vol. 2.
Urbina, J.A., Docampo, R., 2003. Specific chemotherapy of Chagas disease: controversies and advances. Trends. Parasitol. 19, 495–501.

Vainio, M.J., Johnson, M.S., 2007. Generating conformer ensembles using a multiobjective genetic algorithm. J. Chem. Inf. Model. 47, 2462–2474.
Vainio, M.J., Johnson, M.S., 2005. McQSAR: a multiconformational quantitative structure–activity relationship engine driven by genetic algorithms. J. Chem. Inf. Model. 45, 1953–1961.
Vazquez-Chagoyan, J.C., Gupta, S., Garg, N.J., 2011. Vaccine development against *Trypanosoma cruzi* and Chagas disease. Adv. Parasitol. 75, 121–146.
WHO – Word Health Organization, 2008. Chagas Disease: Special Programme for Research and Training in Tropical Disease, TDR..
Yap, C.W., 2011. PaDEL-descriptor: an open source software to calculate molecular descriptors and fingerprints. J. Comp. Chem. 32, 1466–1474.